ISSN 1560-0904, Polymer Science, Series B, 2018, Vol. 60, No. 6, pp. 789–797. © Pleiades Publishing, Ltd., 2018.

FUNCTIONAL POLYMERS

New Microporous Thiophene-Pyridine Functionalized Imine-Linked Polymer for Carbon-Dioxide Capture[1]

Suha S. Altarawneh[a],*,, Taher S. Ababneh[a], Lo'ay A. Al-Momani[a], and Ibtesam Y. Aljaafreh[a]**

[a] *Department of Chemistry and Chemical Technology, Tafila Technical University, Tafila, Jordan*

**e-mail: suha_tarawneh@yahoo.com*

***e-mail: sus.ttu@gmail.com*

Received March 26, 2018;
Revised August 23, 2018

Abstract—The synthesis, porosity and the capability for carbon dioxide gas-capture of functionalized thiophene-pyridine microporous imine-linked polymer synthesized via the Schiff base condensation reaction between (1,3,5-triformyl thienyl benzene) and 2,6-diaminopyridine is described. The structural formation of the polymer was successfully confirmed via ^{13}C NMR (CP-MAS) and IR spectroscopy, and elemental analysis. The polymer has the good thermal stability up to 380°C, a non-defined aggregated particles morphology and amorphous nature. From the argon sorption isotherm at 87 K, the polymer revealed a moderate Brunauer–Emmett–Teller surface area (372 m^2/g) and micro-size pores (~5 Å). The CO_2 uptake was studied at 273 and 298 K to evaluate the polymer tendency for capturing CO_2 from the surrounding atmosphere. At 298 K, the polymer has shown a reversible adsorption-desorption isotherm with significant uptake (11.4 wt %) at 1.0 atm. The binding energy of CO_2 at zero gas coverage is 24 kJ/mol and decreased upon loading.

DOI: 10.1134/S1560090419010019

INTRODUCTION

Conjugated microporous organic polymers (CMPs) are an emerging class of fascinating porous materials constructed from organic units connected in 2D- and or 3D-structural dimensions via covalent bond and possess cavities in the micropore size (<2 nm) [1–4]. The synthesis of CMPs introduced new class of materials of low skeleton density, high chemical stability and large specific surface area that overcome the limitations of the metal organic frameworks (MOFs) [5]. The above-mentioned properties assist in the design of promising polymers in versatile technological applications include catalysis, gas storage and separation, sensing, electric energy transfer, drug delivery, and luminescence applications [6].

Up to date, unlimited examples of multi-functional CMPs such as conjugated organic polymers, covalent organic frameworks [7], polymers of intrinsic microporosity [8], heterocyclic-based porous polymers [9] and hyper-cross linked polymers [6] are synthesized in different structural skeleton and polymerization processes. In recent reports, most of the CMPs are synthesized via the application of the solution-phase polymerization methods including Schiff-base reaction, phenazine ring-fusion reaction, Friedel–Crafts reaction, Suzuki, Yamamoto, Sonogashira coupling reactions, oxidative coupling reaction, and cyclotrimerization reaction [10–12].

Each class of the CMPs and its polymerization process has its own characteristic properties, advantages and limitations. In this work, we have focused on one selective example of CMPs named heterocyclic-based organic polymers (HPPs) synthesized via Schiff base condensation reaction.

The synthetic heterocyclic porous organic polymers are known as a class of conjugated covalent organic polymers that incorporate the heterocycles by direct and indirect functionalization. The direct synthetic technique depends on the formation of the ring upon the polymerization as in the case of imidazole, carbazole, oxazole, and thiazole-based polymers that have been synthesized by Schiff base co-condensation reaction and used for small gas separation application [13–16]. On the other hand, the indirect incorporation of the ring, such as in thiophene, pyridine and triazine, depends on the coupling of the monomers via organic linker as in the benzimidazole- triazine containing polymers and the open-chains: thiophene-pyridine imine-linked polymers [17–19].

[1] The article is published in the original.

Recent report has shown example of the CMPs that are functionalized with thiophenebi-thiophene, terthiophene and all-thiophene-moieties. This class of polymers has been used for manufacturing of semiconductors, light-emitting diodes and photovoltaic due to their selective electrical, redox, photoluminescence, and charge-transport properties [7–12]. It is believed that the atoms in the heterocyclic rings with lone pair electrons, such as N and S in the functionalized groups, may significantly enhance the polymer properties and make it a potential candidate in the environmental applications such as metal ion removal from drinking water and small gas (e.g. CO_2, N_2, CH_4) capture and separation. The inclusion of heteroatoms such as N, S, O in the polymer backbone introduce new basic sites due to non-aromatic, free-lone pair of electrons on the atoms. Also, it is improved the dipole–dipole interaction between the gas molecules and the functionalized polymer surface and facilitate Lewis acid-base interaction between the atom and CO_2 gas [20, 21].

Herein, we have synthesized new microporous thiophene-pyridine bifunctionalized polymer and evaluated the polymer's performance toward CO_2 gas capturing. Furthermore, we have performed DFT calculations to investigate the significant sites for CO_2 capture through polymer simulation and the binding energy of the gas.

EXPERIMENTAL

Materials and Methods

All chemicals were purchased from Sigma-Aldrich and used without further purification, unless otherwise noted. Air-sensitive samples and reactions were handled under nitrogen atmosphere using Schlenk line technique.

^1H and ^{13}C NMR spectra were recorded on a Bruker AVANCE-400 MHz NMR spectrometerin $CDCl_3$ using TMS as an internal reference. CP-MAS solid state NMR measurements were performed at 9.4 Tesla on a Bruker AVANCE 400 spectrometer equipped with double-tuned probes capable of MAS (magic angle spinning). The samples were packed in 3.2 mm rotors made of zirconium oxide spinning at 15 kHz. ^1H-MAS NMR was obtained with single-pulse excitation (90° pulse, pulse length 2.4 μs) and a recycle delay of 6 s. ^{13}C-{^1H}-CP-MAS NMR spectra were acquired using cross polarization (CP) technique with contact time of 3 ms to enhance sensitivity, a recycle delay of 6 s and ^1H decoupling using a TPPM (two-pulse phase modulation) pulse sequence. The spectra are referenced with respect to tetramethylsilaneusing (tetrakis(trimethylsilyl)silane) as a secondary standard (3.55 ppm for ^{13}C, 0.27 ppm for ^1H). Carbon, nitrogen, sulfur, oxygen and hydrogen analysis wasperformed using a Vario EL elemental analyzer. Thermogravimetric analysis (TGA) was carried out using TA Instruments Q-5000IR series thermal gravimetric analyzer with samples held in 50 μL platinum pans under atmosphere of air (heating rate 10 deg/min). Scanning electron microscopy imaging (SEM), were taken on a Hitachi SU-70 scanning electron microscope. IR spectra were recorded on a Shimadzu FT-IR-8300 on KBr pellets in the wavenumber range 4000–400 cm^{-1}. Argon sorption isotherms (at 87 K) and carbon dioxide uptake (at 298 K) were obtained by using a TriStar II 3020 surface area and porosity analyzer (Micromeritics, USA).

Synthesis of 1,3,5-(triformylthienyl)benzene

1,3,5-(Triformylthienyl)benzene (TFTB) was synthesized via Suzuki coupling method according to the reported literature [11, 17]:

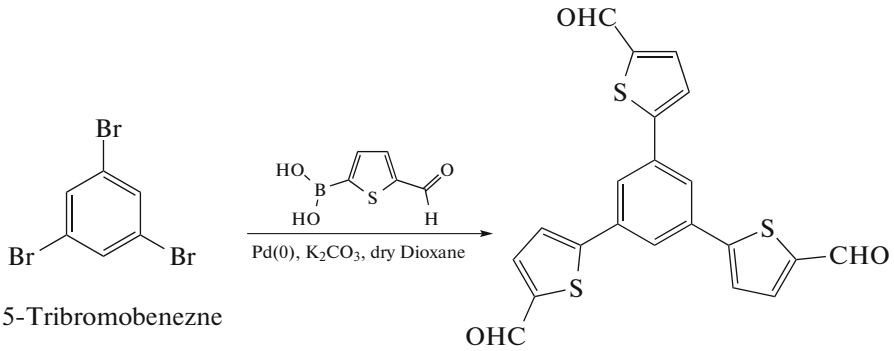

1,3,5-Tribromobenezne

TFTB

A mixture of 1,3,5-tribromo benzene (1.0 g, 3.18 mmol), 4-formylthienylboronic acid (2.98 g, 19.1 mmol), potassium carbonate (2.64 g, 19.1 mmol) and palladium tetrakis(triphenylphosphine) (0.12 g, 1×10^{-4} mmol) and anhydrous 1,4-dioxane (80 mL) under nitrogen atmosphere. The suspension was stirred and refluxed at 85°C for 3 days. The resulting orange suspension was poured into acidic ice slurry

(70 mL HCl/ 200 g ice) and stirred for 30 min. The product was filtered and extracted with chloroform then recrystallized from hot ethylacetate to produce TFTB as yellow product (1.03 g, 80.0%). Anal. Calcd., % for $C_{18}H_{12}O_2S$: C 61.74; H 2.96; O 11.75; S 23.55. Found, %: C 60.99; H 2.78; O 11.50; S 24.37.

Synthesis of Thiophene-Pyridine Imine-Linked Polymer

The thiophene-pyridine imine-linkedpolymer (TPIm) has been synthesized via condensation reaction between TFTB, and 2,6-diaminopyridine according to the reported literature [17]:

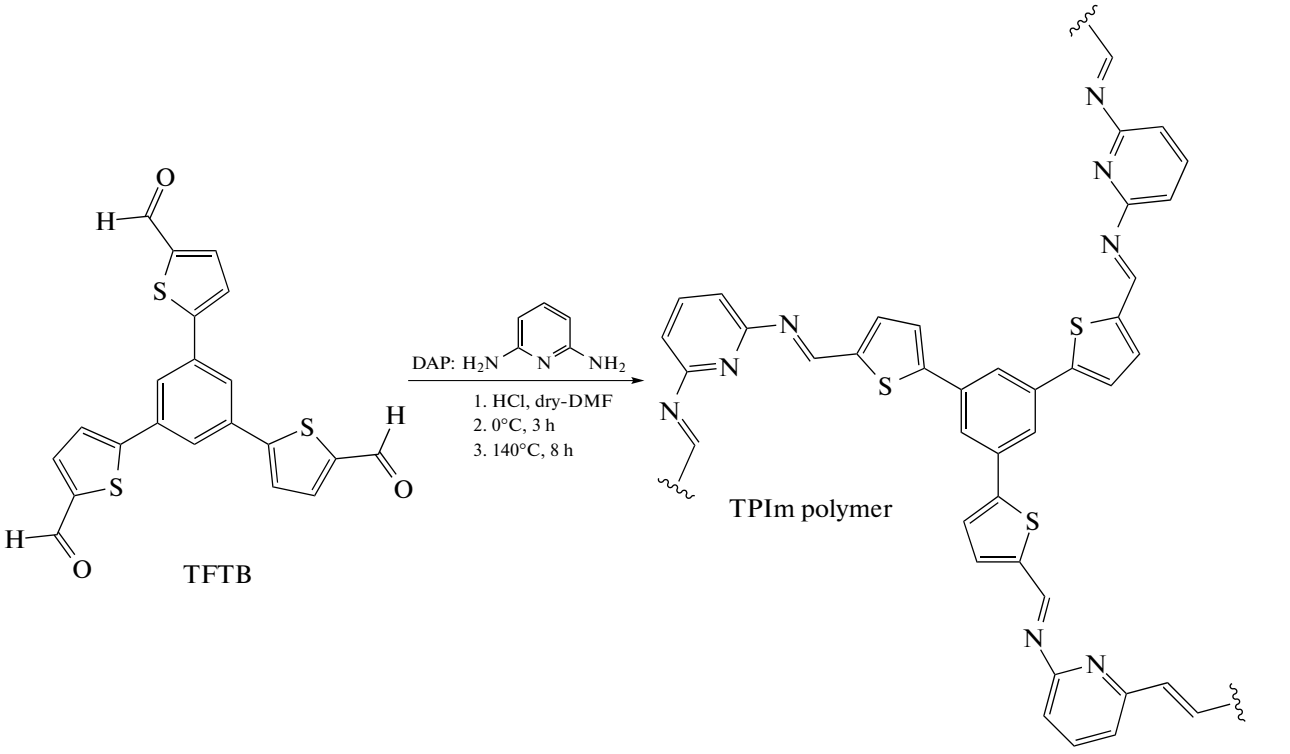

2,6-Diaminopyridine (36 mg, 0.33 mmol) was dissolved in anhydrous DMF (60 mL). The solution was protonated with (2 mL, 2M HCl) and stirred for 2 h at 0°C. In a separate shlenk flask, TFTB (45 mg, 0.11 mmol) was dissolved in anhydrous DMF (40 mL) and stirred for 1 h. The solution of TFTB was added dropwise to the solution of 2,6-diaminopyridine over 3 h while maintaining the temperature of the solution controlled around 0°C. After completion of the addition, the resulted brown suspension mixture was heated up to 140°C for 8 h. The product was filtered and washed with excessive amount of water, 0.1 M HCl, 0.1 M NaOH and acetone, then dried under vacuum for 24 h. (75 mg, 81.0%). Anal. Calcd., % for $C_{16}H_9N_2S$: C 73.54; H 3.47; N 10.72; S 12.27. Found, %: C 73.22, H 3.95; N 10.90, S 11.93.

RESULTS AND DISCUSSION

Synthesis and Physical-Chemical Properties of the Polymer

The purity of the synthesized 1,3,5-(triformylthienyl)benzene was proven by the ^{1}H and ^{13}C NMR (Fig. 1). According to NMR data, no by-product or non-reacted compounds are found. ^{1}H NMR, δ_H, ppm: 9.22 (s, 3H, formyl-H), 7.83 (d, 3H, thienyl-H), 7.60 (d, 3H, thienyl-H), and 7.23 (s, 3H, phenyl-H).^{13}C NMR, δ_C, ppm: 182.5, 148.0, 143.3, 138.0, 134.0, 129.0, and 125.0.

The chemical connectivity and the formation of the imine linker was confirmed by FTIR, elemental analysis and solid-state CP-MAS ^{1}H and ^{13}C NMR. The FTIR spectra of the polymer and its corresponding monomers in the range 4000–400 cm^{-1} are depicted in Fig. 2a. The band at around 3450 cm^{-1} in the spectrum of 2,6-diaminopyridine (DAP) is attributed to the free amine group. The bands in the range 1588–1620 cm^{-1} are related to the imine bond (–C=N–) and the C=N of the pyridine ring. The disappearance of the stretching frequency at 1720–1750 cm^{-1} in the spectrum of the polymer indicates the consumption of the formyl group (CHO) upon condensation. The bands corresponding to the C=C–H, C=C (phenyl ring) and C–S–C (thiophene ring) appear at 3100, 1520 and 1050 cm^{-1}, respectively.

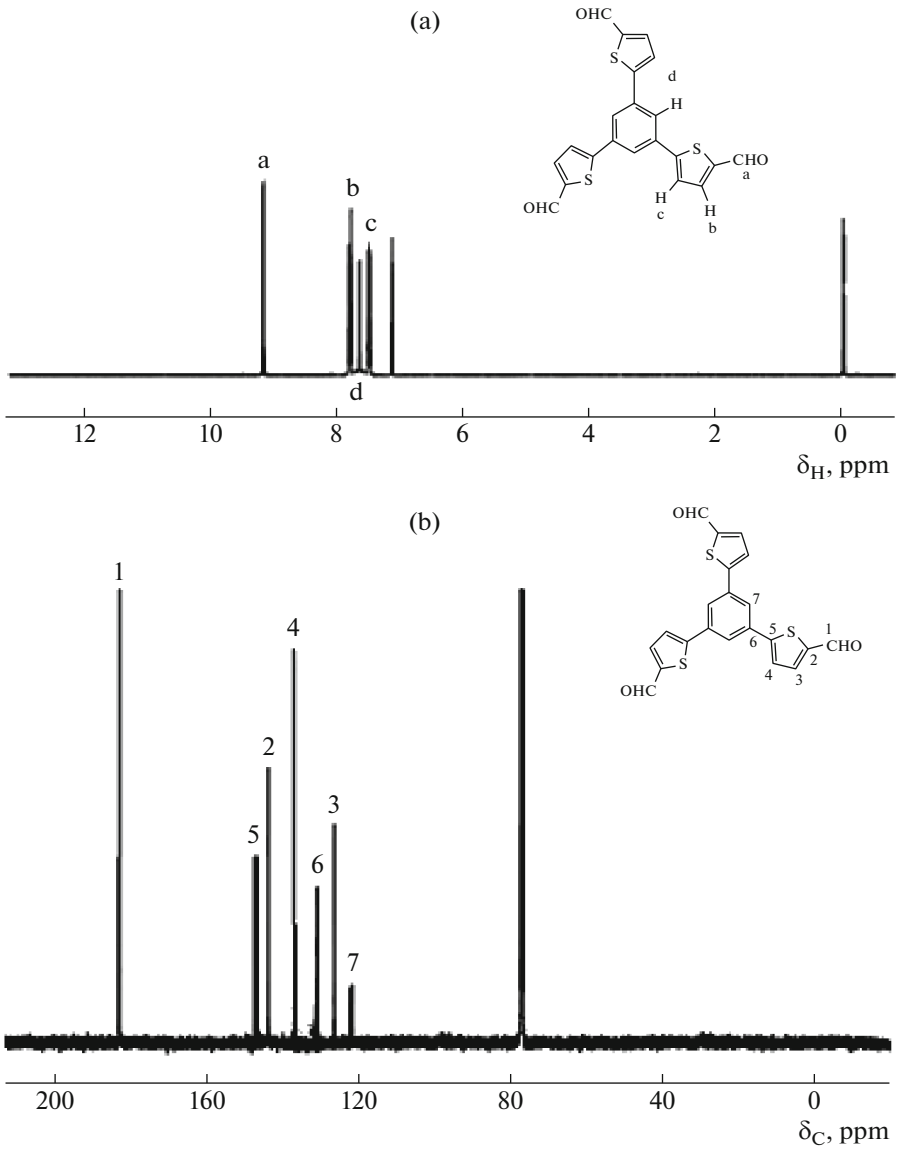

Fig. 1. (a) ^{1}H NMR and (b) ^{13}C NMR of the TFTB measured at 400 MHz, $CDCl_3$.

The ^{13}C NMR CP-MAS spectrum (Fig. 2b) revealed characteristic peaks of the imine and C–S bonds along with other peaks that correspond to the aryl units (phenyl and thienyl carbons) of TPIm. The signals of the carbon (C=C–N–) of pyridine and the imine (–C=N–) appear at 158 and 152 ppm, while the signals at around 144, 140 are ascribed to the thiophene (C–S–C). The signals at 138, 134, 128, 127, 126, and 115 ppm are related to the aromatic carbons of the phenyl, pyridyl and thienyl rings. In contrast, ^{1}H CP-MAS NMR has shown a broad peak due to the overlapped protons of the polymer skeleton and this spectrum is non-informative.

The polymer is thermally stable up to 380°C under N_2 (Fig. 2c). The analysis of the morphology of the polymer revealed a random-size and agglomerated particles ca. 0.5–0.3 mm in size as depicted on SEM image (Fig. 2d). The X-ray diffraction confirmed the amorphous nature (Fig. 3).

Porosity Measurements and Carbon-Dioxide Uptake

The porosity parameters including the surface area, pore size distribution and pore volume of the new conjugated imine-linked polymer PTIm were collected by performing the sorption analysis using argon gas as the sorbate molecule at 1 atm and 87 K (Fig. 4a). The argon adsorption–desorption isotherms are fully reversible with minor hysteresis consistent with the powdery nature of the polymer. The notable rapid argon uptake at very low pressure supports the microporosity nature of the polymer and exhibits the

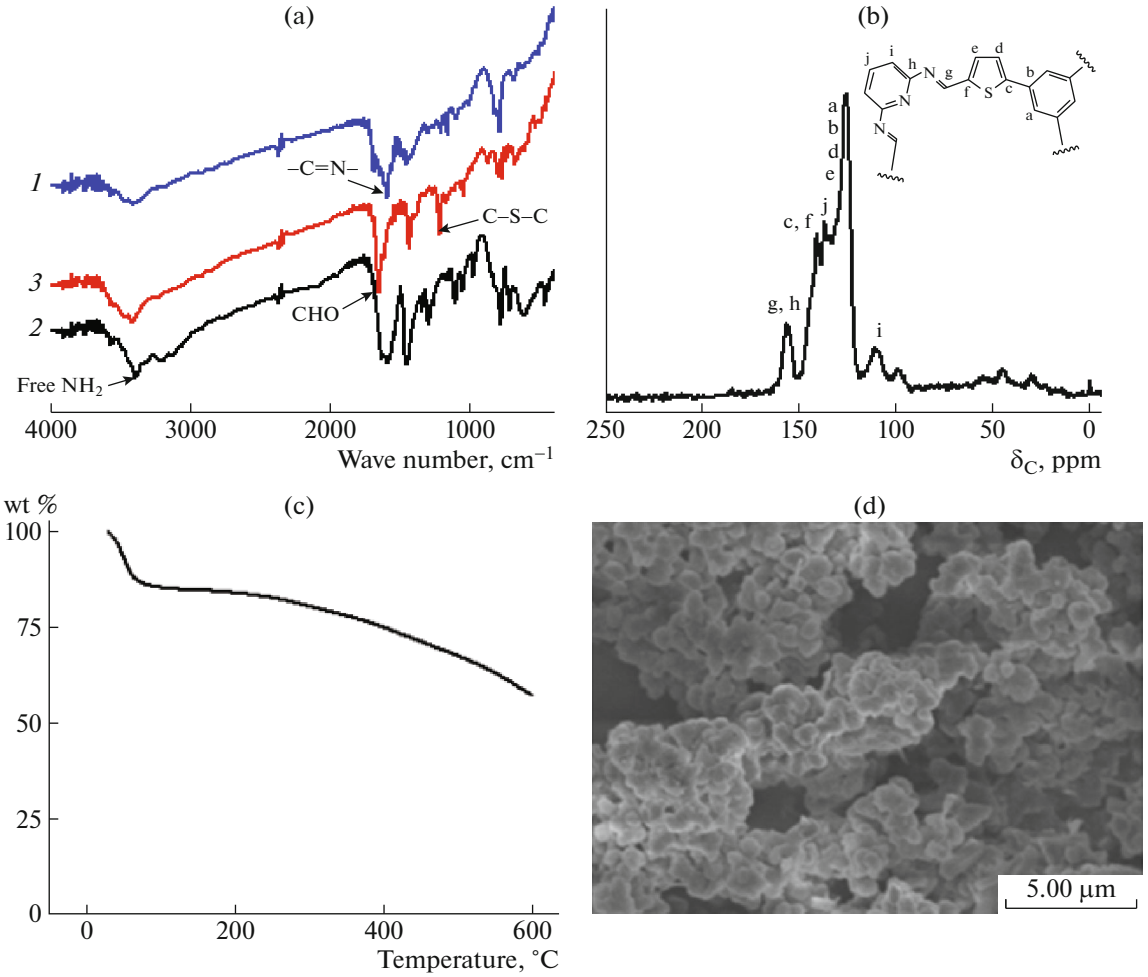

Fig. 2. (Color online) (a) IR spectra of (*1*) the polymer TPIm and corresponding monomers: (*2*) DAP and (*3*) TFTB; (b) ^{13}C CP-MAS solid state of the polymer, (c) the loss weight of the polymer, (d) SEM image of the polymer.

type I isotherm. The surface area of the polymer is an important numerical value, which gives information about the available surface of the polymer for the adsorption process. It can be determined by using the Brunauer–Emmett–Teller (BET) and the Langmuir methods [11]. The BET surface area of the polymer was found to be 372 m^2/g. The Pore size distribution curve derived from the nonlocal density functional theory was found to be centered around 5 Å (Fig. 4b). The pore volume determined at relative pressure ($P/P_0 = 0.97$ atm) is 0.43 cm^3/g. The determined low-to-moderate surface area of the polymer is consistent with the planar, 2-dimentional geometrical structure of the monomers, which assist the π–π stacking and the polymer packing. This in turn decreases the measured porosity and creates a nonsufficient free volume [11, 13, 19]. Another factor that might assist the formation of low-to-moderate surface area, is the rapid polymerization process at room temperature. This factor is built up in according with the two-dimentional imine-Linked and benzimidazole polymers which were polymerized at cryogenic conditions (−60°C) and their surface areas were higher than in PTIm [13, 17].

Environmentally, the polymer capability for capturing carbon dioxide from contaminated air is a vital application of microporous polymers. Thus, and due to the presence of thiophene-pyridine moieties, we have evaluated the polymer performance toward the carbon dioxide capture from a flow of CO_2 gas. As mentioned above, the presence of S and N atoms that possess lone pairs of electrons facilitates a dipole–quadrupole interaction with carbon dioxide molecules as Lewis acid-base interaction [21]. To do so, we have collected CO_2 sorption data at 273 and 298 K at 1 atm. The CO_2 gas uptake isotherms show (114 mg/g, 11.4 wt %) at 273 K and (75 mg/g, 7.5 wt %) at 298 K (Figs. 4c, 4d). The low uptake values are attributed to the modest surface area (372 m^2/g), when compared with other porous polymers. These results are within

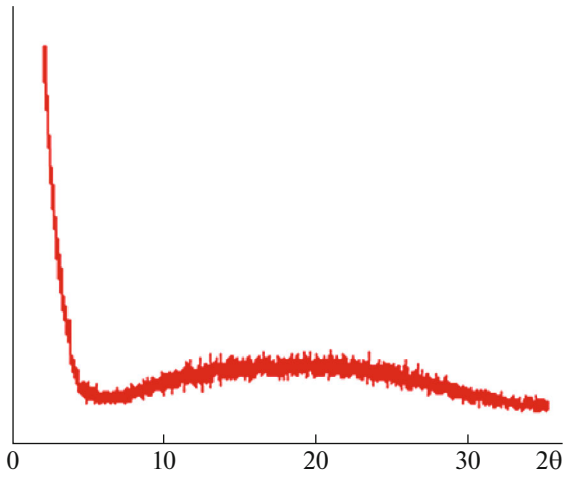

Fig. 3. (Color online) XRD pattern of the polymer.

the range of CO_2 captured gas from moderate surface area polymers such as benzimidazole-, oxazole- and thiazole-based polymers [11, 13, 19].

For determining the binding affinity between CO_2 molecules and the polymer, we have applied the virial method [15] of calculation by using the experimental data of the gas uptake. From the calculations, the binding affinity values are highest at zero coverage (24 kJ/mol) and then drop with higher loading, as shown in Fig. 5.

The initial high binding affinities are driven by favorable interactions between CO_2, the nitrogen and sulfur sites which become less accessible as loading increases. The binding affinity values are consistent with the range of estimated values reported for BILPs [11, 19] and other nitrogen and sulfur functionalized organic polymers [11, 17]. Further calculations were estimated by using density functional theory calculations to gain more insight into the impact of the functionalized surface on CO_2 binding affinity and to determine the effective interaction sites.

Table 1. CO_2 binding energies E_b computed at the M06-2x/6-311+G** level of theory (E_T defines total energy)

CO_2 loading	E_T, kJ/mol	E_b, kJ/mol	E_b, (per CO_2) kJ/mol
TPIm–1CO_2	–3692764.60	–23.00	–23.00
TPIm–2CO_2	–4187888.76	–43.35	–21.68
TPIm–3CO_2	–4683015.60	–66.38	–22.13
TPIm–4CO_2	–5178138.32	–85.29	–21.32

In order to examine the interaction of CO_2 with open binding sites of TPIm, we have undertaken a theoretical investigation involving the building unit of the thiophene-pyridine microporous imine-linked polymer and nCO_2 molecules, (where n = 1, 2, 3 and 4). Several adsorption configurations were considered by allowing the CO_2 molecules to approach the different possible coordination sites of the TPIm building unit. All initial molecular orientations were explored by running a conformer distribution calculation for 10000 conformers at the semiempirical quantum chemical PM6 [22] level of theory. This conformational search was followed by optimization of the 300 minimal-energy conformers at the HF/3-21G then B3LYP/6-31G* [23–28] levels of theory narrowing down the outcome to 30 structures. These structures were then used as inputs and were fully optimized without any geometry or symmetry constraints in the gaseous phase employing DFT calculations at the global hybrid functional M06-2x level of theory with the polarized and diffused 6-311+G** basis set [29].This step is the most demanding in terms of computational resources. The optimized ground-state geometries of TPIm–nCO_2 calculated at the M06-2x/6-311+G** level of theory is illustrated in Fig. 6. The geometries of TPIm–nCO_2 where one, two, three and four CO_2 molecules were allowed to interact with different binding sites of TPIm exhibited configurations where CO_2 is bound to the N-sites of the TPIm. Lengths of the CO_2–N bonds ranged from 2.74 to 2.98 Å and averaged 2.86 Å. Additionally, O atoms of CO_2 was found to bind well with neighboring H atoms of the aromatic system with bond lengths ranging from 2.45 to 2.88 Å and averaging 2.67 Å. This result is consistent with the atomic charges obtained by applying the Natural Bonding Orbital method (NBO) [30].On average, the NBO charge on the C atoms of CO_2 is determined to be +1.055e (range from +1.047 to +1.062e), in contrast to that of the N atoms of the coordination sites at –0.527e (range from –0.486 to –0.558e). Furthermore, the average NBO charge on the O atoms of CO_2 is –0.529e (range from –0.517 to –0.540e), compared to that of the bound H atoms of the aromatic system at +0.213e (range from +0.163 to +0.243e). Bond angle deformation is also accompanied upon coordination of CO_2 with the binding sites of TPIm. A maximum angle reduction value of 3.5° is calculated for the TPIm–1CO_2 building site. A similar deformation is found in the literature in which angle reduction values of 3.1° and 4.0° were reported [31, 32]. By loading more CO_2 molecules into the TPIm building unit, these interactions will have less stabilizing effect and angle reduction becomes less apparent until it reaches a minimum value of 0.9° in TPIm–4CO_2. This behavior is evident from the calculated CO_2 binding affinities E_b where it has been shown that with more CO_2, the binding energy decreases from 23.0 to 21.3 kJ/mol (Table 1). This result is in good

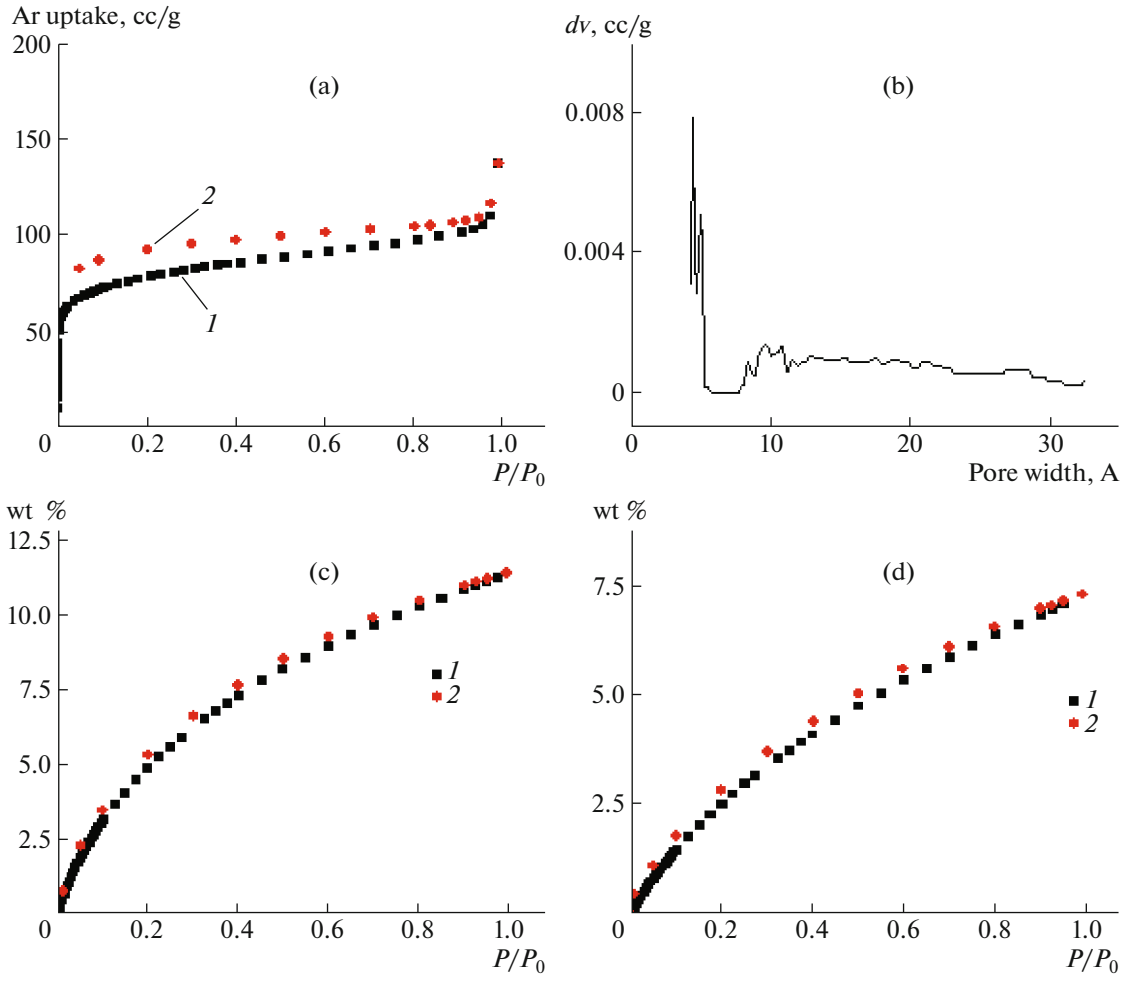

Fig. 4. (Color online) (a) Argon uptake isotherm at 87 K, (b) pore size distribution, (c) CO_2 uptake (wt %) at 273 K, and (d) CO_2 uptake (wt %) at 298 K. (*1*) Adsorption and (*2*) desorption.

agreement with the experimental data where a maximum binding affinity of 24.0 kJ/mol was achieved, representing the energy at zero coverage of the gas. By loading more CO_2, the affinity should decrease since the molecules will then be at a farther distance for interacting with the binding sites.

CONCLUSIONS

To summarize, a new microporous thiophene-pyridine functionalized porous organic polymer (PTIm) with BET surface area 372 m^2/g has been synthesized and characterized. The polymer is microporous and has a tendency of capturing 11.4 wt % at 273 K. The effective available sites for CO_2 attraction have been determined by applying DFT calculations. Overall, the calculations have shown that the gas molecules approach to the sites decorated with S and N.

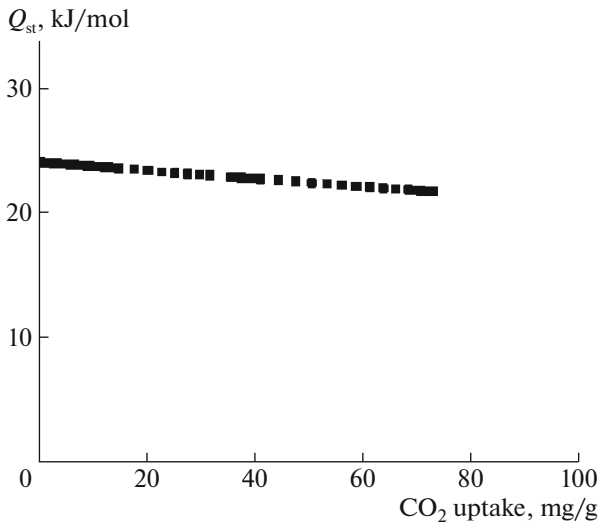

Fig. 5. Binding affinity (Q_{st}) of the loaded CO_2 gas at 298 K.

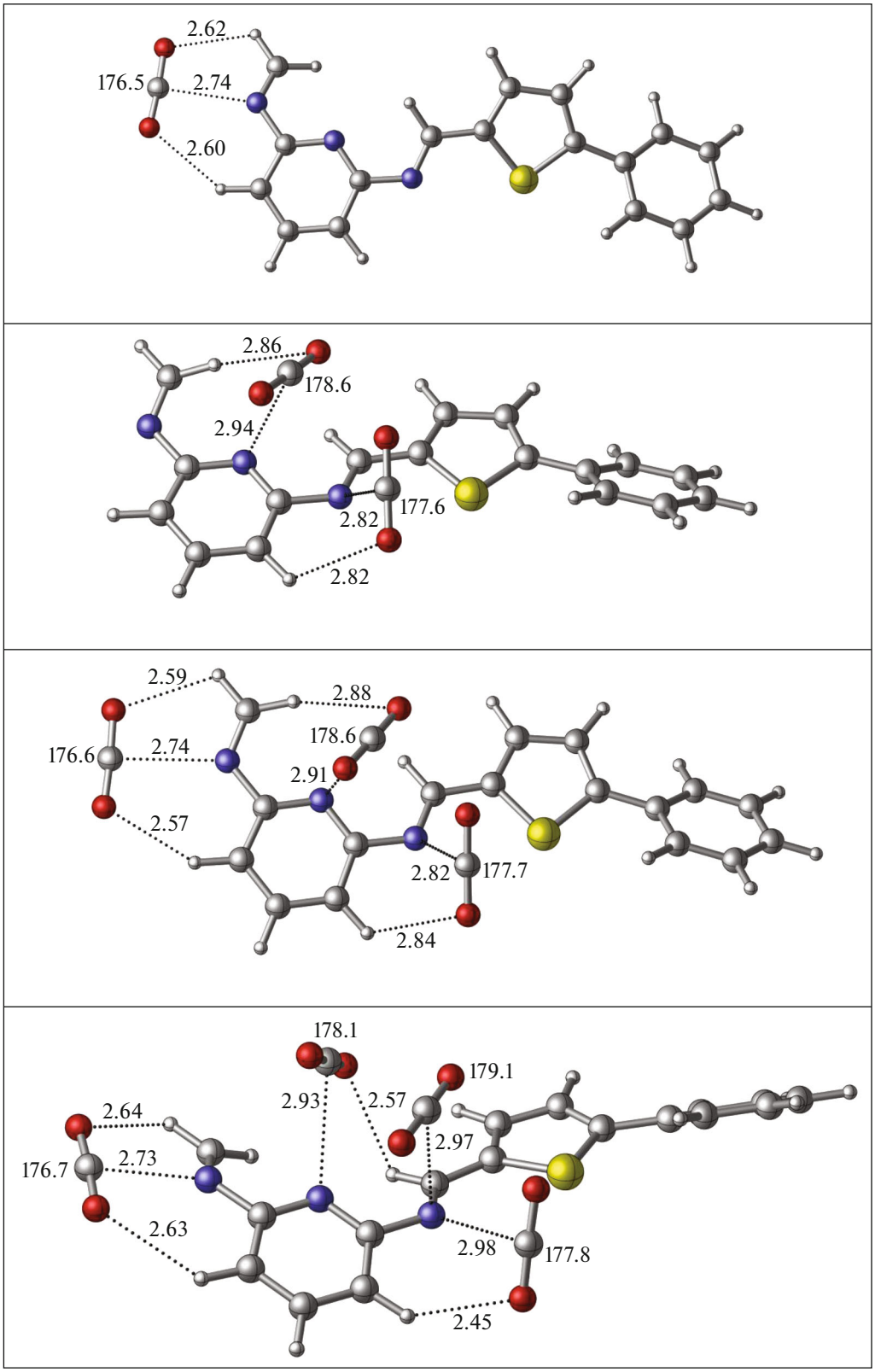

Fig. 6. (Color online) Fully optimized geometries of TPIm–CO_2 interactions calculated at the M06/6-311+G* level of theory.

ACKNOWLEDGMENTS

The authors acknowledge financial support from Tafila Technical University (contract grant number 2015/106). S.T. gratefully acknowledges Prof Hani Elkaderi (VCU-USA) for all his help for learning this area of research during her PhD. The authors, also strongly Thank Dr. Andreas Seifert from Chemnitz University of Technology for the valuable help in the polymer characterizations and CP MAS solid state measurements.

REFERENCES

1. S. Xu, B. Tan, and A. Parthiban, in *Synthesis and Applications of Copolymers* (Wiley, Hoboken, 2014), p. 125.
2. B. Li, Z. Guan, X. Yang, W. Wang, I. Hussain, K. Song, B. Tan, and T. Li, J. Mater. Chem. A **2**, 11930 (2014).
3. R. Dawson, E. Stockel, R. Holst, D. Adams, and A. Cooper, Energy Environ. Sci. **4**, 4239 (2011).
4. Z. Chang, D. Zhang, Q. Chen, and X. Bu, Phys. Chem. Chem. Phys. **15**, 5430 (2013).
5. J. Chun, S. Kang, N, Park, E. Park, X. Jin, K. Kim, H. Seo, S. Lee, H. Kim, W. Kwon, Y. Park, J. Kim, Y. Kim, and S. Son, J. Am. Chem. Soc. **136**, 6786 (2014).
6. L. Tan and B. Tan, Chem. Soc. Rev.**46**, 3322 (2017).
7. C. Diercks and O. Yaghi, Science **3**, 355 (2017).
8. D. Ramimoghadam, E. Gray, and C. Webb, Int. J. Hydrogen Energy **41**, 16944 (2016).
9. C. Sun, P. Wang, H. Wang, and B. Han, Polym. Chem. **7**, 5031 (2016).
10. A. Rengaraj, P. Puthiaraj, Y. Haldorai, N. Heo, S. Hwang, Y. Han, S. Kwon, W. Ahn, and Y. Huh, ACS Appl.Mater. Interfaces **8,** 8947 (2016).
11. S. Altarawneh, S. Behera, P. Jena, and H. El-Kaderi, Chem. Commun. **50**, 3571 (2014).
12. G. Zhu and H. Ren, in *Porous Organic Frameworks: Design, Synthesis and Their Advanced Applications* (Springer, Berlin; Heidelberg, 2015), p. 13.
13. M. Rabbani, T. Islamoglu, and H. El-Kaderi, J. Mater. Chem. A **5**, 258 (2017).
14. W. D. Guerra, R. A. Rossi, A. B. Pierini, and S. M. Barolo, J. Org. Chem. **80**, 928 (2015).
15. E. Wolkenberg, D. Wisnoski, H. Leister, Y. Wang, Z. Zhijian, and W. Lindsley, Org. Lett. **6**, 1453 (2004).
16. N. Joshi, V. Saxena, A. Singh, S. P. Koiry, A. K. Debnath, M. M. Chehimi, D. K. Aswal, and S. K. Gupta, Sens. Actuators, B **200**, 227 (2014).
17. S. Altarawneh, T. Jazzazi, T. Ababneh, T. Al Shboul, and I. Al Jaafreh, J. Appl. Polym. Sci. **134**, 44331 (2017).
18. I. Aljaafreh, S. Altarawneh, M. Alomari, A. Almaabreh, and M. Al Amelat, Indones. J. Pure Appl. Chem. Res. **6**, 34 (2017).
19. S. Altarawneh, T. İslamoğlu, A. Sekizkardes, and H. El-Kaderi, Environ. Sci. Technol. **49**, 4715 (2015).
20. J. Wang, I. Senkovska, M. Oschatz, M. Lohe, L. Borchardt, A. Heerwig, Q. Liu, and S. Kaskel, ACS Appl. Mater. Interfaces **5**, 3160 (2013).
21. H. Sun, X. Zhao, P. Wang, H. Wang, and B. Han, Sci. China: Chem. **60**, 1067 (2017).
22. D. Pyles, W. Crowe, L. Baldwin, and P. McGrier, ACS Macro Lett. **5**, 1055 (2016).
23. J. J. P. Stewart, J. Mol. Model. **13**, 1173 (2007).
24. J. Binkley, J. Pople, and W. Hehre, J. Am. Chem. Soc. **102**, 939 (1980).
25. A. D. Becke, J. Chem. Phys. **98**, 5648 (1993).
26. A. D. Becke, J. Chem. Phys. **104**, 1040 (1996).
27. C. Lee, W. Yang, and R. G. Parr, Phys. Rev. B: Condens. Matter Mater. Phys. **37**, 785 (1988).
28. G. A. Petersson, A. Bennett,T. G. Tensfeldt, M. A. Al-Laham, W. A. Shirley, and J. A. Mantzaris, J. Chem. Phys. **89**, 2193 (1988).
29. G. A. Petersson, T. G. Tensfeldt, and J. A. Montgomery, Jr., J. Chem. Phys. **94**, 6091 (1991).
30. Y. Zhao and D. G. Truhlar, Theor. Chem. Acc. **120**, 215 (2006).
31. E. Reed, R. B. Weinstock, and F. J. Weinhold, J. Chem. Phys. **83**, 735 (1985).
32. K. D. Vogiatzis, A. Mavrandonakis, W. Klopper, and G. E. Froudakis, ChemPhysChem **10**, 374 (2009).